ARCHIVES OF ELECTRICAL ENGINEERING VOL. 71(1), pp. 75–90 (2022)

DOI 10.24425/aee.2022.140198

Research on magnetic regulation characteristics of axial-radial flux type permanent magnet synchronous machine

CUNXIANG YANG[1], KUN WANG[1] ✉, ZIYANG LIU[1], BIN XIONG[2], QIANG ZHAO[3]

[1] *Zhengzhou University of Light Industry*
Zhengzhou, Henan, China

[2] *Institute of Electrical Engineering of Chinese Academy of Sciences*
Beijing, China

[3] *Wolong Electric Nanyang Explosion Protection Group Co., LTD.*
China

e-mail: {yangzzha/✉wangkun/LiuZY}@zzuli.edu.cn, {807123702/1165490915}@qq.com

(Received: 05.06.2021, revised: 20.09.2021)

Abstract: Due to the fixed rotor magnetic field, the main magnetic flux of conventional permanent magnet synchronous motors (PMSMs) cannot be flexibly adjusted. Recently, the axial-radial flux type permanent magnet synchronous machine (ARFTPMSM) based on the hybrid excitation concept is proposed, which provides a new method for the speed and magnetic field regulations for PMSMs. To analyze the mechanism of magnetic field variation inside the ARFTPMSM, in this paper, three – dimensional finite element models for electromagnetic field calculation of the ARFTPMSM are established. On this basis, the influence of the axial device on the motor is discussed, and the mechanism of flux regulation is explained. By the quantitative calculation of air-gap flux density and the no-load back-electromotive force (EMF), the flux regulation capability of the ARFTPMSM is verified. In addition, the effect of the excitation magnetomotive force on the magnetic field harmonics is analyzed combined with the winding theory, and the influence of the axial magneto-motive force (MMF) on the torque fluctuation is obtained. The flux regulation performance of the motor and the validity of the numerical calculation analysis are verified by the experiments.

Key words: ARFTPMSM, axial excitation device, flux regulation capability, HEM

1. Introduction

Permanent magnet synchronous motors (PMSMs) are widely used in many areas for their high-power density, high efficiency, and good reliability [1]. Nowadays, many methods, such as vector control, saliency ratio optimization, have been studied and adopted to improve the efficiency and the speed control performance of PMSMs [2–5].

Hybrid excitation machines (HEMs), which have combined the advantages of PM machines and wound field machines, are recently proposed. The HEM has two excitation sources, the main magnetic field consists of the electric excitation magnetic field and the permanent magnetic field, the air-gap flux can be regulated by excitation control efficiently [6–8].

Due to the simple and direct adjustment method of the HEM, the independent adjustment and control of the air gap magnetic field can be realized [9, 10]. At present, the HEM has broad prospects in the fields of wind power generation, electric vehicles, and aerospace, and also has become a hotspot in the field of motor research [11, 12].

A new topology of a parallel hybrid excitation machine (PHEM) is proposed in [13], which combines a permanent magnet synchronous motor (PMSM) and a doubly salient electromagnetic machine (DSEM), providing a solution for improving its magnetic field regulation capacity.

In reference [14], an optimized HESM with a magnetic shunt rotor is proposed, and an optimized control strategy is proposed by using the coordinated operation of excitation current and d-axis current.

At present, many HEMs have over-complicated structures and are difficult to manufacture, which has a large limitation on wide applications. The axial-radial flux type permanent magnet synchronous machine (ARFTPMSM) based on the principle of flux adjustment of the HEM improves the traditional PMSM, simplifies the manufacturing process, and makes use of the remaining space at both ends of the stator.

The purpose of this study is to discover the variation mechanism of the main magnetic field, the relationship between the flux density distribution and the flux adjusting range, and the effect of axial excitation flux on magnetic field harmonics.

In this paper, by using the time-stepping finite-element method, a 3.5 kW ARFTPMSM is taken as the prototype to establish a three-dimensional finite element model. Firstly, the influence of the axial excitation device on the motor, and the mechanism of flux regulation are analysed. The influence of the axial excitation magnetomotive force (MMF) on the no-load back-EMF and the air-gap flux density is studied by the quantitative analysis, the range of flux adjusting is determined. Then, by the calculation of winding factor of different harmonics, combined with the Fourier decomposition method, the different nonlinear variations of each magnetic field harmonics with the axial MMF are clarified, further, the variation of torque fluctuation is investigated. Finally, the accuracy of finite element calculation is verified by experiments. The research can provide a reference for the development of HEMs.

2. Structure and working principle of ARTFPMSM

The ARFTPMSM consists of three parts: the stator part, the rotor part, and the axial excitation part. The stator part is similar to the fractional slot concentrated winding interior PMSM. Unlike the conventional PMSM, the axial excitation part is added to both sides of the motor. The axial

excitation part is composed of the end cap and the axial flux exciting windings, in order to make the axial magnetic circuit closed, the machine end cap (1 in Fig. 1) with certain magnetic conductivity has been designed, the axial flux exciting windings are fixed in the slots of the rings of the end cap.

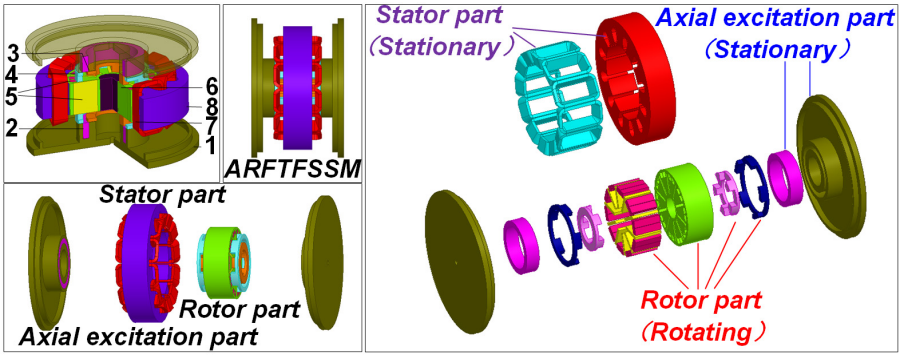

Fig. 1. Structure of ARTFPMSM: 1 – end cap; 2 – axial excitation coil; 3 – S pole ferromagnetic bridge; 4 – N pole ferromagnetic bridge; 5 – permanent magnets; 6 – rotor core; 7 – armature windings; 8 – stator core

The motor structure is shown in Fig. 1, basic parameters are listed in Table 1.

Table 1. Basic parameters of the ARFTPMSM

Parameter	**Value**	**Parameter**	**Value**
Stator out diameter (mm)	230	Rated power (kW)	3.5
Stator inner diameter (mm)	140	Rated speed (r/min)	250
Iron core axial length (mm)	50	Slot number	12
Radial air gap length (mm)	0.5	Pole number	10
Axial air gap length (mm)	0.5	Number of parallel branches	1
		Winding connection type	Y

To provide an axial magnetic circuit to communicate the rotor part and the excitation part, the ferromagnetic bridges are used, and are placed on both rotor sides. The structure of the N ferromagnetic bridge and S ferromagnetic bridge is shown in Fig. 2. At the sides of the ferromagnetic bridges which near the rotor are designed as claw pole structures, and are directly connected with the rotor, the number of magnetic teeth corresponds to the machine pole pairs. Each ferromagnetic bridge corresponds to one kind of rotor magnetic pole, to ensure that the magnetic flux in the axial magnetic circuit flows in a single direction.

Figure 3 shows the construction of the rotor. The permanent magnets include radial permanent magnets and tangential permanent magnets. This hybrid permanent magnet arrangement can

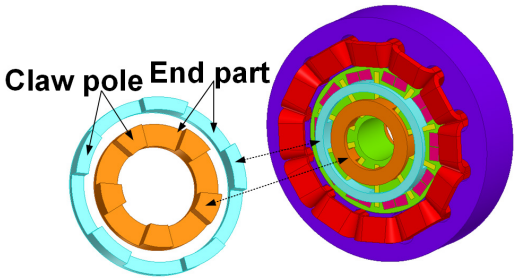

Fig. 2. Structure of ferromagnetic bridge

enhance air gap magnetic flux density and increase the overload capacity of the motor. In addition, the tangential permanent magnet makes the N-pole and S-pole in the rotor separate, a magnetic short-circuit is avoided, which is beneficial for the axial flux to adjust the main flux through the claw pole of the ferromagnetic bridge.

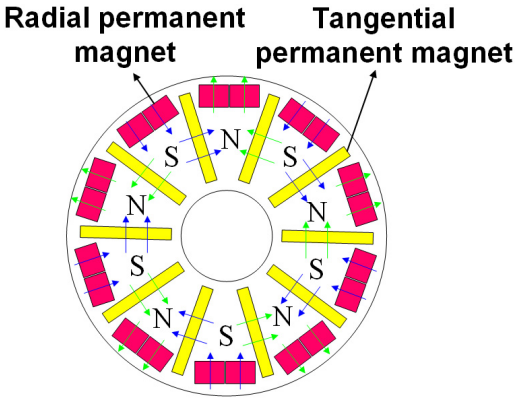

Fig. 3. Structure of rotor

The stator core is equipped with fractional slot concentrated windings. By adopting this structure, the direct axis inductance of the motor can be increased and the flux regulation ability will be improved.

Unlike the conventional PMSM, axial excitation devices are added at both ends of the ARFTPMSM. The end cap consists of two concentric ferromagnetic rings and an endplate, the axial exciting windings are placed between ferromagnetic rings, constant direct current is fed into the excitation coil to produce an axial magnetic flux. The axial excitation part does not rotate with the rotor, a gap referred to as the axial air gap exists between the axial excitation part and the rotor.

To calculate and analyze the axial magnetic field, the 3-D electromagnetic field model was established by the time-step finite element method. The motor structure and the 3-D finite element mesh model are shown in Fig. 4.

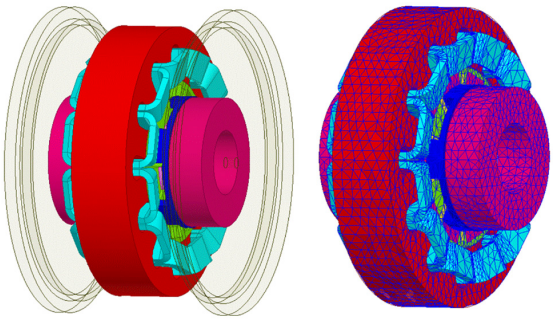

(a) (b)

Fig. 4. The 3-D model of ARTFPMSM: (a) motor structure; (b) the mesh model

To simplify the calculation in electromagnetic analysis, the following hypothesis was proposed:

1. Harmonics caused by the external controller are not considered, only the harmonics caused by the structure of the motor are considered.
2. Materials are isotropic.
3. The influences of the temperature on material conductivity and permeability are ignored.

The rotor needs excellent axial magnetic conductivity so that the magnetic flux could flow in the axial direction and adjust the main magnetic field. In order to ensure the mechanical strength and axial magnetic permeance of the rotor, the rotor material is magnetic steel (m20) and the rotor is designed as a solid structure. The ferromagnetic bridge serves as the bridge connecting the electrical excitation flux and the permanent magnet flux, and plays an important role in the axial magnetic circuit. Therefore, the ferromagnetic bridge needs good axial permeability, so the m20 is also used.

Figure 5 shows the working principle of the ARFTPMSM. As shown in Fig. 5(a), when there is no excitation current in the axial excitation coil, only the magnetomotive force generated by the

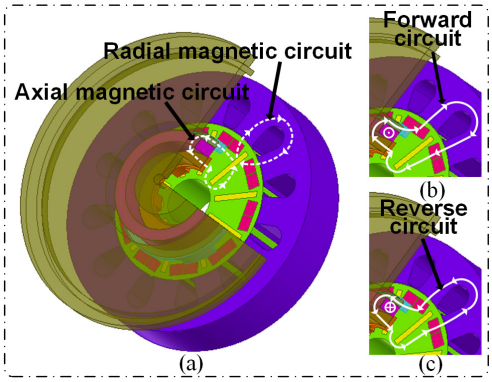

Fig. 5. Working principle of the ARFTPMSM: (a) permanent magnet magnetic circuit; (b) forward current magnetic circuit; (c) reverse current magnetic circuit

permanent magnet exists in the motor, and the flux will flow through both the axial magnetic circuit and radial magnetic circuit. The axial magnetic circuit starts from the N pole of the permanent magnet and returns to the S pole of the permanent magnet through the N-pole ferromagnetic bridge, the axial air gap, the end cap, the axial air gap, and the S-pole ferromagnetic bridge.

As shown in Fig. 5(b), when the current of the axial excitation coils is in the forward direction, the axial excitation device will produce the axial MMF, the axial flux passes through the ferromagnetic rings, the axial air-gap, the N pole ferromagnetic bridge, the rotor, the radial air-gap, and the stator, then returns to the radial air-gap, the S pole ferromagnetic bridge, the axial air-gap, the ferromagnetic ring, and the magnetic circuit is closed through the end cap.

As shown in Fig. 5(c), when the current of the axial excitation coils is in the reverse direction, the flux generated by the axial excitation device flows through the path consistent with that in Fig. 5(b), but in the opposite direction.

3. Analysis of the magnetization mechanism

3.1. Effect of axial excitation device on ARFTPMSM

From the foregoing, the axial excitation device can not only generate axial excitation MMF to regulate the magnetic field but also change the flow path of permanent magnet flux. Figure 6 shows the influence of the axial excitation device on the magnetic flux density vector of the rotor, and the air gap magnetic flux density of the ARFTPMSM is calculated.

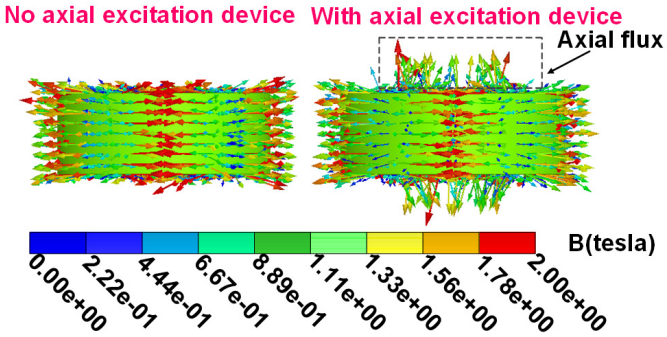

Fig. 6. Magnetic flux density vectors when axial device is used

Figure 7 shows the three-dimensional distribution of air gap magnetic flux density when the motor is on no-load. It can be seen that the radial air gap magnetic flux density in the axial direction is evenly distributed.

It can be seen from the figure that the magnetic flux distribution in the axial direction is uniform. For better analysis, the mean values of radial air gap magnetic flux density are obtained, the axial magnetic density distribution with and without the axial device is compared in Fig. 8(a). The no-load back-electromotive force (EMF) is also an important index to reflect the change of the magnetic field of the motor. Figure 8(b) combines the variations of air gap magnetic flux density and the no-load back EMF.

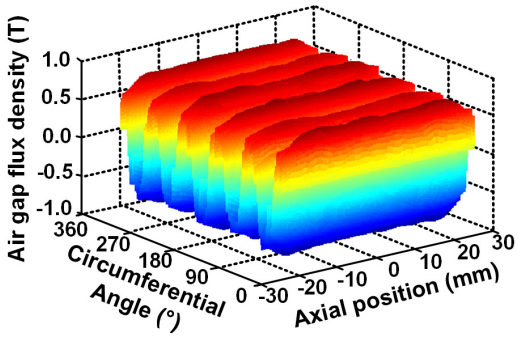

Fig. 7. The three dimensional distribution of flux density

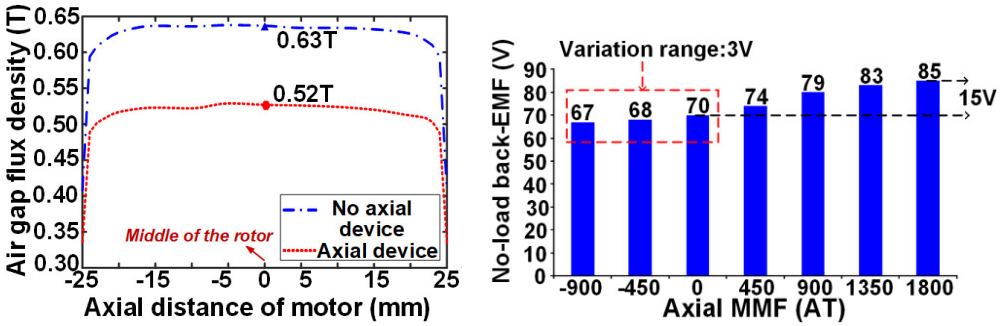

(a) (b)

Fig. 8. Effect of axial device on the magnetic field of the motor: (a) air gap flux density in axial length; (b) average magnetic flux density and back-electromotive force

It can be seen from the figure that the magnetic flux distribution in the axial length of the rotor is uniform, but there is abrupt attenuation at the ends of the rotor, which is caused by the leakage flux flowing into the axial magnetic circuit. As can be seen from the figure, in the middle of the rotor core, the air gap flux density is reduced by 0.11 T when the axial excitation is used, and the no-load back EMF is also decreased by 13 V.

3.2. Analysis of magnetic adjustment characteristics

When the current with different amplitude and direction flows through in the axial excitation windings, different MMFs will be produced, and the main magnetic field of the motor can be regulated through the axial magnetic circuit. To analyse the mechanism of ARFTPMSM flux regulation, the flux density vector of the rotor and ferromagnetic bridge under different axial MMF is compared.

As can be seen from Fig. 9, when the axial excitation MMF is 0 AT, the excitation device does not produce magnetic flux, a part of the magnetic flux produced by the permanent magnet flows into the ferromagnetic bridge, so that the air gap magnetic flux will be reduced, and the motor is

working in the flux weakening region. When the axial MMF is –900 AT, the axial magnetic flux density vector on the ferromagnetic bridge increase. This is because the reverse axial MMF is consistent with the direction of the PM axial flux and opposite to the direction of the PM radial flux, which can enhance the axial magnetic field and weaken the radial magnetic field.

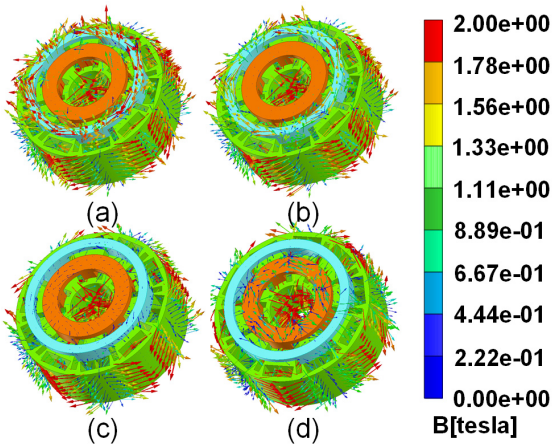

Fig. 9. Magnetic flux density vector distribution when axial MMF is different: (a) –900 AT; (b) 0 AT; (c) 900 AT; (d) 1800 AT

With the increase of the axial MMF, the axial magnetic flux shows an increasing trend, while the main magnetic flux decreases gradually. When the axial MMF increases to 900 AT (as shown in Fig. 9(c), the axial magnetic flux flowing into the ferromagnetic bridge by the permanent magnet has counteracted the axial excitation flux, the flux density vector on the ferromagnetic bridge is small.

As shown in Fig. 9(d), when the axial MMF is 1800 AT, it can be seen that the direction of axial magnetic flux is opposite to that in Fig. 9(a) and Fig. 9(b). The direction of the axial excitation flux is consistent with the radial magnetic circuit of the permanent magnet flux and opposite to the axial magnetic circuit of the permanent magnet flux, the radial magnetic field is enhanced and the axial magnetic field is weakened.

To analyze the magnetic regulation performance, the air gap flux density of the motor in the axial direction is obtained when the axial magnetomotive force is different, the variation of flux density is shown in Fig. 10. When the axial MMF is lower than –900 AT or higher than 1800 AT, the change of air gap magnetic flux density is very small and can be ignored.

As can be seen from the figure, when the axial MMF is negative, the radial air gap magnetic flux density is weakened, and the range of weakening is 0.02 T. When the axial MMF is positive, the radial gap magnetic flux density is enhanced, the enhancement range is 0.14 T, the regulating range of the forward flux is 7 times that of the reverse flux.

The variation of no-load back EMF is consistent with the change of flux density. When the axial MMF is negative, the no-load back EMF will decrease, and the range of variation is 3 V. When the axial MMF is positive, the no-load back EMF will rise, and the range of variation is 15 V.

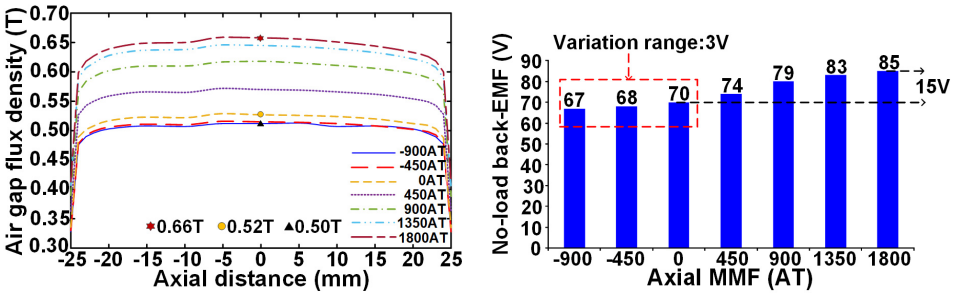

(a) (b)

Fig. 10. (a) Air gap magnetic density distribution under different axial MMF; (b) no-load back EMF under different axial MMF

4. Analysis of ARFTPMSM'S magnetic regulation performance

4.1. Harmonic analysis of air gap magnetic field

Due to the use of fractional slot concentrated windings, the magnetic field is rich in harmonic components, the axial flux will affect the harmonics of the main magnetic field to different degrees, which will be an important factor affecting the motor performance.

In order to better analyze the effect of axial flux on the main magnetic field of the motor, the main harmonics inside the motor are clarified by calculating the winding coefficients and the effect of axial flux is further studied.

According to Formula (1), the winding factor of each harmonic is calculated and listed in Table 2.

$$K_{dpv} = K_{dv} K_{pv} \,. \tag{1}$$

Formula 2 shows the short short-pitch factor K_{pv} of the v-th harmonic

$$K_{pv} = \sin\left(\frac{vp\alpha_s y_1}{2}\right), \tag{2}$$

where: v is the order of the harmonic, $\alpha_s = 2\pi/Q_s$ is the slot torque angle, y_1 is the pitch, q is the number of pole-pairs.

The calculation method of the distribution coefficient K_{dv} of the motor with double-layer fractional slot concentrated windings motor is different from that of an integer slot motor, and the method is shown in Formula (3) [15].

$$K_{dv} = \begin{cases} \dfrac{\sin\left(\dfrac{\pi}{2m}\right)}{\dfrac{q_{ph}}{2}\sin\left(\dfrac{a_{phv}}{2}\right)}, & \text{when } q_{ph} \text{ is even}, \quad v = \dfrac{(2n-1)t}{p},\ n = 1,2,3\ldots \\ \dfrac{\sin\left(\dfrac{\pi}{2m}\right)}{q_{ph}\sin\left(\dfrac{\alpha_{phv}}{4}\right)}, & \text{when } q_{ph} \text{ is odd}, \quad v = \dfrac{nt}{p},\ n = 1,2,3\ldots \end{cases}, \tag{3}$$

where m is the number of phases and t is the number of the unit motor.

$$q_{ph} = \frac{Q}{mt}$$

is the number of slots per pole, per phase of the unit motor.

$$\alpha_{phv} = \frac{2\pi}{Q_s/t}\left(1 + \delta_{ph}\frac{v \cdot p - p}{t}\right)$$

is the electrical angle between adjacent phasors in the groove electromotive force star diagram.

$$\delta_{ph} = \frac{kQ_s/t + 1}{p/t},$$

where k is the smallest integer that makes δ_{ph} an integer.

Table 2. Winding factors of different harmonics

Harmonic order	**1/5**	**3/5**	**1**	**7/5**	**9/5**	**11/5**
K_{dpv}	0.067	–0.25	0.933	0.933	–0.25	0.067

As can be seen from Table 2, the winding factor of 7/5-th harmonic is large and the same as that of the fundamental wave, which has the greatest impact on the motor performance.

In order to analyse the variation of radial air gap magnetic density under the influence of axial excitation flux, the finite element method is used for numerical calculation in the presented paper. The air gap magnetic density is decomposed by the Fourier transform, and the variation of the magnetic field harmonics in the radial air gap is further discussed. Ignoring the high-order harmonic components, the magnetic flux density fundamental wave and each harmonic are shown in Fig. 11. It can be seen from Fig. 11, the value of 7/5-th harmonic is the largest.

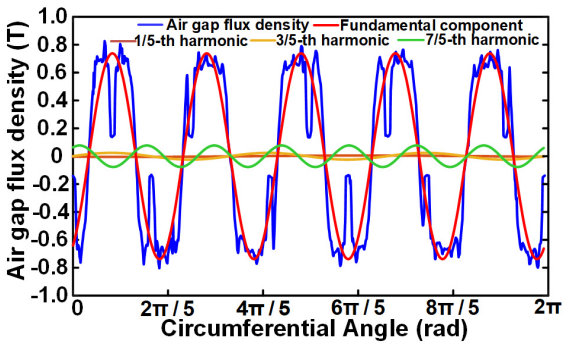

Fig. 11. Radial air gap magnetic density decomposition at no load

Figure 12 shows the variation of fundamental component of flux density under different axial MMF. It can be seen from the figure that the change of the fundamental wave is consistent with that of the axial excitation MMF.

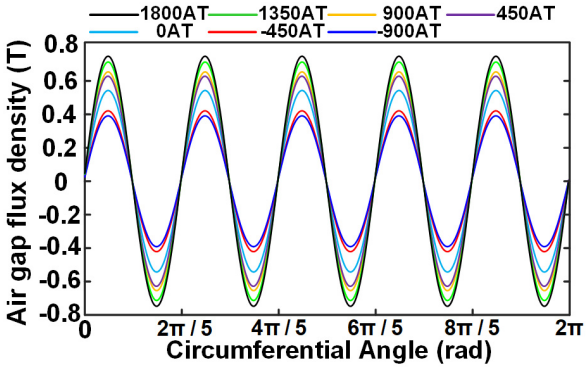

Fig. 12. Variation of fundamental wave under different axial MMF

It can be known from Fig. 13 that the influences of the axial MMF on different harmonics are also different, the variation range of the 7/5-th harmonic is larger than that of the 3/5-th harmonic. When the axial MMF is 0 AT, the amplitude of 7/5-th harmonic is the largest. When the axial MMF is 1800 AT, the amplitude of 3/5-th harmonic is the largest.

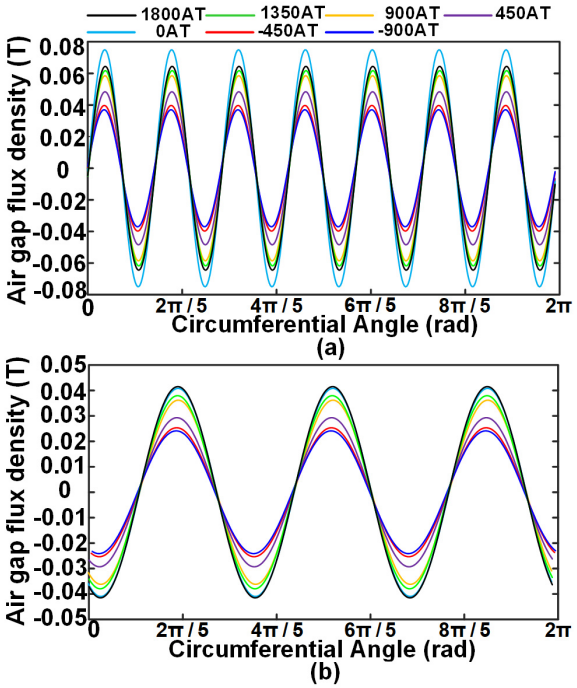

Fig. 13. Variation of flux density harmonics under different axial MMF: (a) 7/5-th harmonic; (b) 3/5-th harmonic

4.2. Analysis of torque fluctuation

The stability of output torque is an important performance of permanent magnet synchronous motors. However, due to the existence of axial magnetic circuits, the harmonic components show different nonlinear variations with the change of the axial magnetomotive force, the torque ripple is also affected when axial excitation MMF is different. The torque fluctuation coefficient can be calculated by Formula (4) in a single cycle [16].

$$K_{mb} = \frac{T_{\max} - T_{\min}}{T_{\max} + T_{\min}} \times 100\%, \tag{4}$$

where: $T_{\max}$ and $T_{\min}$ are the maximum and minimum instantaneous torque in a single cycle; K_{mb} is the torque ripple coefficient.

Figure 14 shows the torque calculated by using the finite element method (FEM). It can be seen from the figure that, when the axial MMF is 0 AT and 1800 AT, the torque fluctuation is relatively small, and when the axial MMF is 900 AT, the torque fluctuation coefficient is the largest, reaching 15.2%.

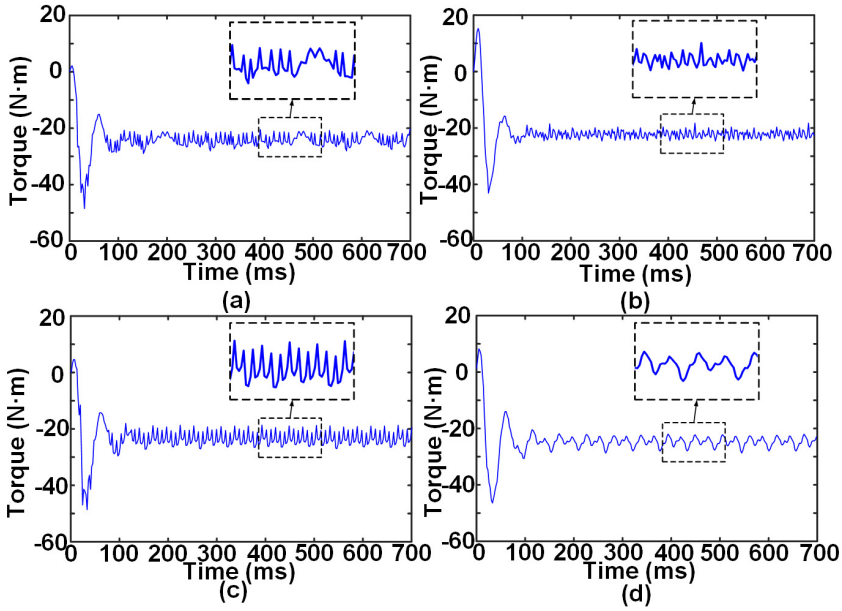

Fig. 14. Torque under different axial MMF: (a) –900 AT; (b) 0 AT; (c) 900 AT; (d) 1800 AT

Table 3 lists the torque fluctuation coefficient of the motor under different axial MMFs. Torque fluctuation coefficient under different axial excitation MMF.

With the increase of reverse axial MMF, the torque fluctuation increases gradually. And with the increase of positive axial MMF, the torque fluctuation first increases, but when the axial MMF exceeds 900 AT, the torque fluctuation coefficient shows a decreasing trend.

Table 3. Torque fluctuation coefficient of the motor under different axial MMFs

Axial MMF	Torque ripple coefficient (%)
–900 AT	11.1
–450 AT	9.3
0 AT	10.9
450 AT	12.3
900 AT	15.2
1350 AT	9.5
1800 AT	9.5

5. Experimental verification

In order to verify the accuracy of the finite element calculation, the motor is tested. The change of air gap flux density can be reflected by the change of no-load back EMF, so in order to get the performance of flux regulation, the no-load back EMF of the motor is measured. Figure 15 and Fig. 16 show the ARTFPMSM prototype and experimental platform, respectively. The no-load

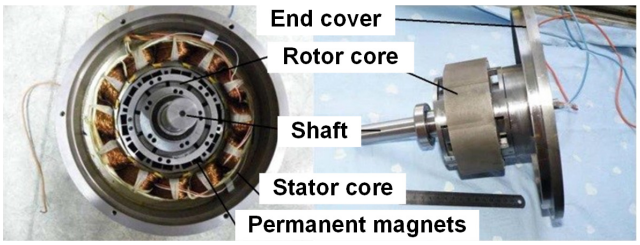

Fig. 15. The ARTFPMSM prototype

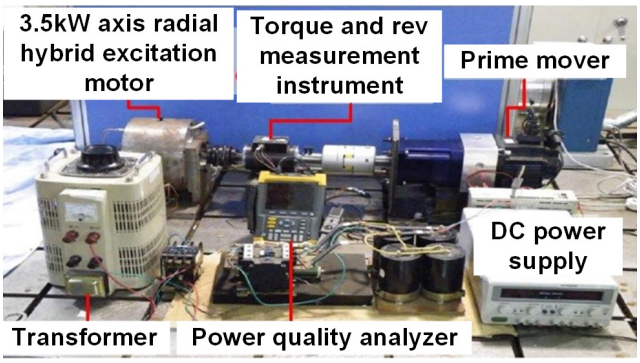

Fig. 16. The experiment platform

back EMF of the prototype under different axial MMF was obtained by dragging the prototype with a speed of 250 rad/s.

It can be known that with the increase of the slot wedge permeability, the eddy current distribution on the cage bars is more uniform, the maximum eddy current density is also reduced.

Figure 17 shows the experimental data measured by the power quality analyser. It should be noted that the voltage data measured by the power quality analyser is line voltage and the voltage calculated by the finite element is phase voltage. Table 4 shows the comparison between the experimental data and the calculated data. The relative error is less than 5%, which is within the reasonable range.

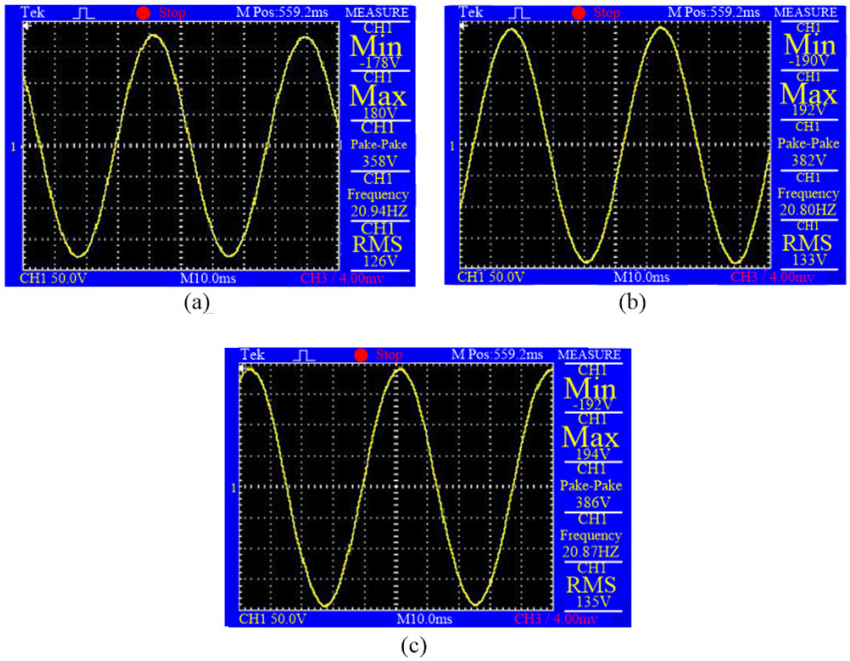

Fig. 17. Line voltage waveforms of the ARFTPMSM: (a) Axial MMF of 0 AT; (b) Axial MMF of 900 AT; (c) Axial MMF of 1350 AT

Table 4. The comparison of measured data and calculated results

Excitation current (A)	**No-load back EMF (phase voltage)**	
	experimental data (V)	**FEM data (V)**
0	73.09	70
6	78.98	80
9	79.80	83
10	80.21	84

6. Conclusions

In this paper, taking a 3.5 kW axial-radial flux type permanent magnet machine (ARFTPMSM) as an example, the mechanism of flux regulation is introduced, and the effect of axial MMF on magnetic adjusting ability is investigated. And the influence of the axial MMF on the magnetic field harmonics and the torque fluctuations are analyzed. The conclusions are as follows:

1. When the axial excitation device is adopted, the magnetic flux generated by the permanent magnet will enter the axial magnetic circuit, and the radial air gap magnetic field will be weakened. Compared with the case that without the axial device, the no-load back EMF of the motor is reduce by 15.48%.
2. When the axial excitation device is used to regulate the magnetic field, the maximum and minimum values of air gap flux density can reach 0.66 T and 0.5 T, respectively. The enhancement range of flux density is 7 times that of the weakening range.
3. The change of flux density fundamental component is consistent with that of axial excitation flux. But the variation of different harmonics influenced by axial flux is also different. Among all magnetic field harmonics, the 7/5-th harmonic has the largest winding factor, and the largest variation range influenced by axial flux. When the axial MMF is 0 AT, the amplitude of 7/5-th harmonic is the highest. When the axial MMF is 1800 AT, the amplitude of 3/5-th harmonic is the highest.
4. As the axial magnetic flux changes, the motor torque fluctuation also changes. When the axial excitation MMF is 0 AT, the motor torque fluctuation is minimum, which value is 9.3%. The torque fluctuation gradually increases when the reversing excitation MMF increases, When the excitation MMF is –900 AT, the torque fluctuation is 11.1%. The torque fluctuation increases and then decreases when the forward excitation MMF increases. When the excitation MMF is 900 AT, the torque fluctuation is the largest, 15.2%.

Acknowledgements

This work was supported in part by the National Natural Science Foundation of China under Grant U2004183, 51507156, in part by the Science and Technology Research Project of Science and Technology Department of Henan Province under Grant 202102210100 and 202102210104, and in part by the Foundation for Key Teacher of Henan Province 2018GGJS087.

References

[1] Hongbo Qiu, Xifang Zhao, Cunxiang Yang, Ran Yi, Yanqi Wei, *Influence of permanent magnet parameters on output performance of a High-speed permanent-magnet generator*, IEEJ Transactions on Electrical and Electronic Engineering, vol. 14, no. 8, pp. 1254–1261 (2019), DOI: 10.1002/tee.22925.

[2] Zhang L., Fan Y., Lorenz R., Cui R., Li C., Cheng M., *Design and analysis of a new five-phase brushless hybrid-excitation fault-tolerant motor for electric vehicles*, IEEE Trans. Ind. Appl., vol. 53, no. 4, pp. 3428–3437 (2017), DOI: 10.1109/TIA.2017.2685359.

[3] Yıldırız E., Önbilgin G., *Comparative study of new axial field permanent magnet hybrid excitation machines*, IET Electric Power Applications, vol. 11, no. 7, pp. 1347–1355 (2017), DOI: 10.1049/iet-epa.2016.0860.

[4] Jang D., *Problems Incurred in a Vector-Controlled Single-Phase Induction Motor, and a Proposal for a Vector-Controlled Two-Phase Induction Motor as a Replacement*, IEEE Transactions on Power Electronics, vol. 28, no. 1, pp. 526–536 (2013), DOI: 10.1109/TPEL.2012.2199772.

[5] Liu Y., Zhang Z., Wang C., Geng W., Wang H., *Electromagnetic Performance Analysis of a New Hybrid Excitation Synchronous Machine for Electric Vehicle Applications*, IEEE Transactions on Magnetics, vol. 54, no. 11, pp. 1–4 (2018), DOI: 10.1109/TMAG.2018.2841656.

[6] Gao Y., Li D., Qu R., Fan X., Li J., Ding H., *A novel hybrid excitation flux reversal machine for electric vehicle propulsion*, IEEE Trans. Veh. Technol., vol. 67, no. 1, pp. 171–182 (2018), DOI: 10.1109/TVT.2017.2750206.

[7] Zhang Z., Ma S., Dai J., Yan Y., *Investigation of hybrid excitation synchronous machines with axial auxiliary air-gaps and non-uniform airgaps*, IEEE Trans. Ind. Appl., vol. 50, no. 3, pp. 1729–1737 (2014), DOI: 10.1109/TIA.2013.2282937.

[8] Li L., Cao J., Kou B., Yang S., Pan D., Zhu H., *Design of Axial and Radial Flux HTS Permanent Magnet Synchronous Motor's Rotor*, IEEE Transactions on Applied Superconductivity, vol. 20, no. 3, pp. 1060–1062 (2010), DOI: 10.1109/TASC.2010.2042939.

[9] Mbayed R., Salloum G., Monmasson E., Gabsi M., *Hybrid excitation synchronous machine finite simulation model based on experimental measurements*, IET Electric Power Applications, vol. 10, no. 4, pp. 304–310 (2016), DOI: 10.1049/iet-epa.2015.0473.

[10] Weili L., Hongbo Q., Ran Y., Xiaochen Z., Liyi L., *Three-Dimensional Electromagnetic Field Calculation and Analysis of Axial–Radial Flux-Type High-Temperature Superconducting Synchronous Motor*, IEEE Trans. Appl. Superconductivity, vol. 23, no. 1, pp. 5200607 (2013), DOI: 10.1109/TASC.2012.2232923.

[11] Aoyama M., Noguchi T., Motohashi Y., *Proposal of self-excited wound-field magnetic-modulated dual-axis motor for hybrid electric vehicle applications*, IET Electric Power Applications, vol. 12, no. 2, pp. 153–160 (2018), DOI: 10.1049/iet-epa.2017.0285.

[12] Hua H., Zhu Z.Q., *Novel parallel hybrid excited machines with separate stators*, IEEE Trans. Energy Convers., vol. 31, no. 3, pp. 1212–1220 (2016), DOI: 10.1109/TEC.2016.2553149.

[13] Amara Y., Hlioui S., Ahmed H.B., Gabsi M., *Power Capability of Hybrid Excited Synchronous Motors in Variable Speed Drives Applications*, IEEE Transactions on Magnetics, vol. 55, no. 8, pp. 1–12 (2019), DOI: 10.1109/TMAG.2019.2911599.

[14] Geng W., Zhang Z., Jiang K., Yan Y., *A New Parallel Hybrid Excitation Machine: Permanent-Magnet/Variable-Reluctance Machine with Bidirectional Field-Regulating Capability*, IEEE Transactions on Industrial Electronics, vol. 62, no. 3, pp. 1372–1381 (2015), DOI: 10.1109/TIE.2014.2348936.

[15] Weili L., Wang Jing, Xiaochen Z., Kou Baoquan, *Loss calculation and thermal simulation analysis of high-speed PM synchronous generators with rotor topology*, 2010 International Conference on Computer Application and System Modeling (ICCASM), Taiyuan, pp. 612–616 (2010), DOI: 10.1109/ICCASM.2010.5622209.

[16] Bianchi N., Dai Prè M., Luigi Alberti, *Theory and Design of Fractional-Slot PM Machines*, CLEUP, Padova (2007).